ACCOUNTING FOR DIRECTIVITY-INDUCED PULSE-LIKE GROUND MOTIONS IN BUILDING-PORTFOLIO SEISMIC LOSS

M. Fuentes[(1)], R. Gentile[(2)], C. Galasso[(3)]

[(1)]*Research Assistant, Dept. of Civil, Environmental & Geomatic Engineering, University College London, UK, matthias.alziary.18@ucl.ac.uk*

[(2)]*Marie Curie Senior Research Fellow, Dept. of Civil, Environmental & Geomatic Engineering, University College London, UK, r.gentile@ucl.ac.uk*

[(3)]*Associate Professor, Dept. of Civil, Environmental & Geomatic Engineering, University College London UK, and Scuola Universitaria Superiore (IUSS) Pavia, Italy, c.galasso@ucl.ac.uk*

Abstract

Earthquake-induced pulse-like ground motions are often observed in near-source conditions due to forward-directivity. Recent worldwide earthquakes have emphasized the severe damage potential of such pulse-like ground motions. This paper introduces a framework to quantify the impact of directivity-induced pulse-like ground motions on economic losses for building portfolios. To this aim, a simulation-based probabilistic risk modelling framework is implemented for various synthetic building portfolios located either in the fault-parallel or fault-normal orientations with respect to an ideal strike-slip fault. Those portfolios consist of two building typologies representative of distinct vulnerability classes in the Mediterranean region: non-ductile moment-resisting reinforced concrete (RC) frames with masonry infills, mainly designed to sustain gravity loads (i.e. pre-code frames); and ductile moment-resisting RC infilled frames designed according to the Eurocode 8 (EC8) seismic provisions for high ductility class (i.e. special-code frames). Monte Carlo-based probabilistic seismic hazard analysis (PSHA) is first performed, specifically modifying conventional PSHA to account for the pulse-occurrence probability and for the spectral amplification due to near-source directivity effects. Hazard curves for sites/buildings located at different distances from the fault are obtained, and the spatial distribution of the spectral amplification is investigated and critically discussed. A set of pulse-like ground motions and a set of spectrally-equivalent ordinary records are used to perform non-linear dynamic analysis (NLDA) and derive fragility relationships for index buildings representative of each considered building class. A vulnerability model is finally built by combining the derived fragility relationships with a (building-level) damage-to-loss model specifically calibrated for Italy. Results of the study are presented in terms of average annual loss (AAL) for various portfolios of different sizes. These results show that the influence of near-source directivity effects is significant when estimating losses of individual buildings or small portfolios located very close to a fault. Nevertheless, the impact of pulse-like ground motions on losses for larger portfolios can be considered minimal and can be neglected in most of the practical large-scale seismic risk assessment applications.

Keywords: probabilistic risk modelling; directivity-induced pulse-like ground-motion; reinforced concrete frames; building portfolios.

1. Introduction

In near-source (NS) conditions, the spatial configuration of a site with respect to the fault and the rupture propagation can favour the constructive interference of seismic waves. This results in ground motions characterized by a large, full-cycle velocity pulse at the beginning of the record, which concentrates most of the radiated seismic energy. This phenomenon is called forward-directivity, and the resulting ground motions are labelled as “pulse-like”.

In the past, extensive damage observed on structures located in NS regions has been associated to pulse-like ground motions. Examples include events such as the 1999 M7.6 Chi-Chi earthquake, the 1994 M6.7 Northridge earthquake, and most recently, the 2009 M6.3 L’Aquila, and the 2011 M6.1 Christchurch earthquakes. The distinct features of these ground motions and their (potentially) devasting impact on structures have boosted various engineering seismology/earthquake engineering studies over the years

investigating directivity-induced pulse-like ground motion occurrence, features, and their impact on structures [1–3].

Most of the conventional ground motion models (GMMs) used in probabilistic seismic hazard analysis (PSHA) do not explicitly account for the occurrence of directivity-induced pulse-like ground motions and their features (e.g. pulse period), which could lead to an under-prediction of the seismic hazard (e.g. in terms of spectral accelerations) for NS conditions, and could impact the subsequent seismic demand/damage/loss assessment. Some researchers have proposed modifications to the conventional PSHA framework to model the pulse-occurrence probability, the pulse period, and the spectral amplification induced by forward-directivity effects [4–6].

Similarly, for the fragility/vulnerability assessment of buildings in NS regions, a number of studies have addressed the impact of the characteristics of pulse-like ground motions on structural response and consequent damage [7–9]. However, most of these studies are focused only on the collapse assessment of individual buildings, and none of them has addressed loss estimation for NS conditions, particularly when looking at building portfolios. It is worth noting that in the context of this study, fragility refers to the probability of reaching or exceeding a number of damage states conditional on a set of intensity measure -IM- levels, while vulnerability refers to the probability distribution of loss ratio (e.g. asset repair cost as a percentage of the asset replacement cost) at a number of IM levels [10].

This study aims to fill these gaps by investigating the influence of directivity-induced pulse-like ground motions on the estimation of seismic losses for building portfolios, using simulation-based NS-PSHA and a catastrophe risk modelling framework [11]. Quantifying the potential impact of earthquakes-induced pulse-like ground motions on portfolios of properties located in seismically prone regions is of primary interest to property owners, (re-)insurance companies, capital lending institutions, local government agencies, and structural engineers. Each is likely to have a different viewpoint and different (refinement) requirements and can cope with seismic risk using a variety of strategies (e.g. proactive seismic retrofit, earthquake insurance coverage, catastrophe bonds). Regardless of which risk reduction or risk transfer mechanism is ultimately chosen, it is critical that the estimates of potential loss on which these decisions are based are as accurate as possible given the available information.

The study starts with a brief overview of the methodology implemented to account for directivity-induced pulse-like ground motions in building-portfolio seismic loss estimation. The proposed methodology relies on a simulation-based approach to NS-PSHA accounting for pulse-occurrence probability, pulse period, and resulting ground-motion intensities for two case-study (synthetic) building portfolios. The same assessment is carried out using a traditional PSHA framework and the results, in term of hazard curves, are compared and discussed. Non-linear dynamic analysis (NLDA) is performed for two archetype buildings representative of the building classes making the considered portfolios. NLDA employs two sets of ground-motion records: one only including pulse-like ground motions and one including only ordinary (non-pulse-like) records. Fragility relationships for pulse-like and non-pulse-like records are then obtained for various structure-specific damage states and used to derived vulnerability relationships. Finally, average annual loss (AAL) values for different sizes of the considered portfolios - characterized by their maximum distances from the fault - are calculated, and the results are critically discussed.

1.1 Existing models/frameworks for NS-PSHA

The following sub-sections briefly review the modifications introduced in the conventional PSHA framework to account for near-source directivity effects, focusing mainly on the contribution of Chioccarelli and Iervolino [6], which is the NS-PSHA framework used in the illustrative application presented in this paper.

1.1.1. Pulse-occurrence probability

Baker [12], among others, proposed an algorithm for identifying large-velocity pulses in the fault-normal component (i.e. perpendicular to the strike of the fault) of ground-motion records, as forward-directivity effects are generally observed most strongly in the direction orthogonal to the strike. Out of the 3,500 strong ground motions contained in the Next Generation Attenuation (NGA) project library [13], the study found 91 ground motions containing strong velocity pulses and identified the associated pulse period (T_p). Iervolino and Cornell

[14], based on the previous work of Somerville et al. [1] and the pulse-like ground motions identified by Baker [12], proposed a set of models to estimate the probability of pulse occurrence for strike-slip (SS) and dip-slip (DS) events in the fault-normal orientation, depending on the relative location of the site with respect to the source. Eq. (1) is the general form of the model proposed for SS events; it shows that the occurrence probability of pulse-like records depends largely on the site-to-source geometry. The geometric parameters defined by the authors include the minimum distance between the site and the fault (R), the distance between the epicentre and the intersection point between the fault projection and the line of minimum distance from the site (s), the angle between the epicentre and the site with respect to the fault direction (θ). The parameters α and $\beta_{1,2,3}$ correspond to regression coefficients.

$$P(pulse|R,s,\theta) = \frac{e^{\alpha+\beta_1 R+\beta_2 s+\beta_3\theta}}{1+e^{\alpha+\beta_1 R+\beta_2 s+\beta_3\theta}} \tag{1}$$

1.1.2. Pulse period

Chioccarelli and Iervolino [6] performed a linear regression using the pulse-like ground motions identified by Baker [12] and proposed a lognormal model to estimate T_p as a function of the moment magnitude of the event, M_w, following the approach taken previously by other authors [12,15]. Eq. (2) provides the natural logarithm of T_p as a function of M_w with a standard deviation of 0.59 for the residuals.

$$\ln(T_p) = -6.19 + 1.07M_w \tag{2}$$

1.1.3. Amplification of spectral accelerations for pulse-like ground motions

Baker [27] investigated the amplification of spectral accelerations (Sa) of pulse-like ground motions around the pulse period (referred hereafter as spectral amplification) by removing the velocity pulse from the ground motions and comparing the response spectra of the original records and those of the residual ones (with the velocity pulse removed from them). The response spectra were also compared with the spectral acceleration values predicted by using the Boore and Atkinson GMM [16], finding that the responses of pulse-like records are significantly higher than those predicted by the GMM around the velocity pulse period T_p.
Based on these findings, the author proposed an approach to account for such a spectral amplification when predicting the Sa for a structure subjected to a pulse-like ground motion:

1. Compute the spectral acceleration of the residual ground motion using a GMM (that doesn't explicitly account for pulse-like ground motions);
2. Account for the pulse-like spectra amplification by adding the gaussian function $e^{-\left(\ln\left(\frac{T_p}{T}\right)\right)^2}$ to the mean prediction $\mu_{\ln(S_a)_{GMM}}$.

The equations that describe the procedure proposed by Baker are the following:

$$\mu_{\ln(S_a(T))} = \mu_{\ln(Sa)_{GMM}} + e^{-\left(\ln\left(\frac{T_p}{T}\right)\right)^2} \tag{3}$$

$$\sigma_{\ln(S_a)} = \sigma_{\ln(Sa)_{GMM}} \tag{4}$$

2. Simulation-based seismic loss assessment

The methodology implemented in this study to estimate the portfolio losses considering directivity-induced pulse-like ground motions is schematically illustrated in Fig. 1. Specifically, this study considers a portfolio of N_{bldg} buildings, each one characterized by a specific location within the portfolio, a given building class,

and a stochastic catalogue of N_{events} earthquakes, each one corresponding to a given rupture scenario. To estimate the effects of the *j-th* event on the *i-th* building, N_{sim} simulations are generated to account for the uncertainties in the estimation of variables such as the pulse occurrence, pulse period, and resulting spectral accelerations (i.e. the considered IM). In other words, a particular value is generated for those variables for the *k-th* simulation of the *j-th* event affecting the *i-th* building (realization (i, j, k)).
If pulse-like ground motions are not accounted for, a conventional (simulation-based) PSHA framework is used and the pulse-occurrence probability, the pulse-period values, and resulting spectral amplifications are not considered in the simulation process. In this case, the NPL loss (non-pulse-like loss) is calculated for each realization (i, j, k) using the spectral accelerations obtained from conventional GMMs (leading to NPL spectral acceleration) and the fragility curves obtained for ordinary ground motions (NPL fragility curves).
In the case of pulse-like ground motions, a (simulation-based) NS-PSHA framework is used: each realisation (i, j, k) is categorised as pulse-like or non-pulse-like depending on the pulse-occurrence probability of the event *j-th* at the *i-th* building location. If the realisation is categorized as non-pulse-like, the loss is estimated following the conventional PSHA framework (i.e. a NPL loss value will be obtained, as introduced above); if the realization is categorized as pulse-like, the spectral acceleration is calculated considering the spectral amplification (PL spectral acceleration), and the fragility curves obtained for pulse-like ground motions (PL fragility curves), which depend on the T_p/T ratio (see section 3), are used to estimate the PL loss (pulse-like loss).
The results shown in this study hereafter will be named either "far-field" (FF) if they were obtained using a conventional PSHA framework and NPL fragility curves (disregarding the pulse-occurrence probability), or "near-source" (NS) if the NS-PSHA framework and both NPL and PL fragility curves were used. It is worth highlighting that this terminology is only used for convenience as it should be clear that not all the events generated in near-source conditions will be pulse-like.

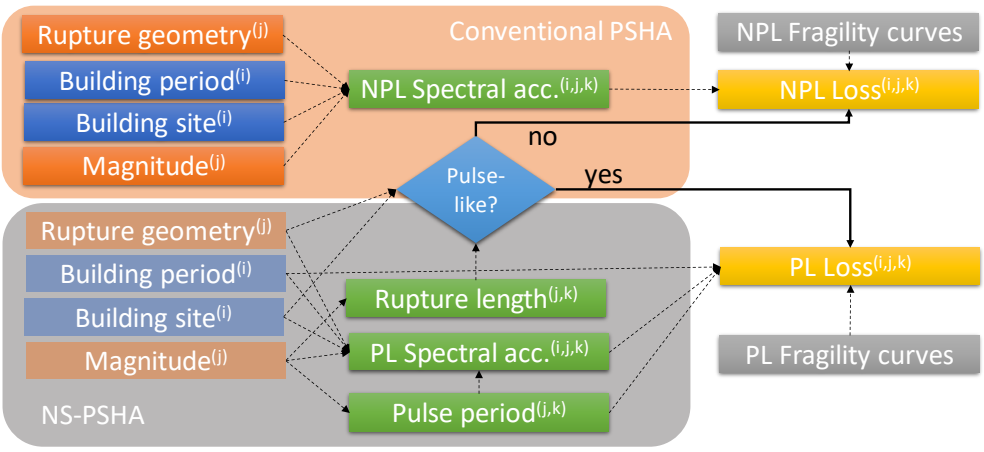

Fig. 1 – Flowchart highlighting dependencies between the variables involved in the calculation of seismic losses for a building portfolio

2.1 Simulation-based NS-PSHA

The conventional PSHA and the NS-PSHA carried out in this study employ a Monte Carlo-based approach [17] to account for the uncertainties in all the factors affecting the ground shaking at a given site. A synthetic set of potential earthquake ruptures is developed by generating random samples for the magnitude, rupture geometry/hypocentre location, and event occurrence time, using relevant probability distributions.
The generated catalogue has a duration of 5,000 years, which is deemed appropriate for the scope of this paper. For each rupture scenario, 500 realizations are generated for the variables of interest (e.g. pulse occurrence, pulse period, and spectral accelerations). To account for near-source directivity effects in the NS-PSHA framework, the set of equations proposed by Chioccarelli and Iervolino [6] is chosen to estimate the pulse probability of occurrence for each site and each event (Eq. 1), the pulse period (Eq. 2) and spectral

amplification (Eq. 3) factor for each realization. The sole GMM used in this study is the one proposed by Boore and Atkinson [16] and only the combined uncertainty, σ_T, is considered for the assessment, with no consideration of ground-motion spatial correlation. Indeed, NS-PSHA would require a spatial correlation model that is explicitly developed for near-fault effects. The use of a spatial correlation model disregarding near-fault effects may mask the actual spatial distribution of ground motion in the vicinity of the fault. To the authors' knowledge, there is no such spatial correlation model that explicitly accounts for the near-fault effects. The reader should consider this fact while implementing the proposed approach for the assessment of hazard in the close proximity of faults. More in general, it is worth highlighting that the focus of this study is on presenting the methodology for the simulation-based NS-PSHA and loss assessment and to perform a comparative analysis in terms of loss results (for pulse-like vs ordinary ground motion) rather than providing absolute loss values.
The results from the NS-PSHA are shown in terms of hazard curves (i.e. annual rate of exceedance vs. Sa values), and they are compared to the results from the conventional PSHA to evaluate the amplification of the spectral accelerations (and its spatial distribution) obtained for different return periods when the pulse-occurrence probability is taken into account.

2.2 Loss assessment

Seismic losses are obtained using the spectral acceleration values from each simulation (as discussed above), the corresponding fragility curves (NPL or PL; see Section 3) and the damage-to-loss model proposed by Di Pasquale et al. [18] as modified by Aljawhari et al. [19], specifically calibrated for Italy. More refined, component-based loss estimation approaches are available (e.g. [20]), although generally targeted for single-building applications. Such approaches are generally deemed unfeasible for large portfolio applications due to the scarcity of input data and the high computational burden.
The results of the analysis are presented in terms of AAL, one of the key outputs of a probabilistic catastrophe risk model. Exceedance probability (EP) curves (i.e. annual probability of exceedance of any loss level) are also computed but not presented here for the sake of brevity. The AAL can be derived directly from the EP curve and represents the expected loss per year (statistical mean loss). The AAL, often referred as the pure premium or 'burn cost', is used as an estimate of the annual insurance premiums to cover the peril [21], and can be calculated by numerically integrating the EP curve or simply by summing up and obtaining the average value of the annual losses from the stochastic catalogue. In this work, the AAL for the *i-th* building is calculated according to Eq. 5, where t_{max} is the time period of the catalogue (i.e. 5,000 years) and N_{events} and N_{sim} are the total number of events of the catalogue and number of simulations per event, respectively (introduced above). The AAL value for the entire portfolio (or part of it) is obtained just by adding up the AAL values of the individual buildings.

$$AAL_i = \frac{1}{t_{max} \cdot N_{sim}} \sum_{j=1}^{N_{events}} \sum_{k=1}^{N_{sim}} loss^{(i,j,k)} \tag{5}$$

3. Impact of pulse-like records on building fragility

To estimate the portfolio losses in NS conditions accounting for forward-directivity effects, fragility curves for ordinary records (NPL fragility curves) and for pulse-like ground motions (PL fragility curves) are required. Both sets of fragility curves are obtained in this study by performing incremental dynamic analysis (IDA) [25] using advanced OpenSees structural models. In particular, two sets of 192 spectrally equivalent (i.e. with similar 5%-damped elastic pseudo acceleration spectra) ground motions are used: the first set is composed by ordinary (non-pulse-like) records, while the second one only contains pulse-like accelerograms. The two sets were assembled by Kohrangi et al. [22], who identified the pulse-like ground motions by means of the algorithm based on wavelet theory, first proposed by Baker [12] and then improved by Shahi and Baker [23]. The authors identified 192 pulse-like ground motions from the NGA-West2 database [24] and 192 companion ordinary records which were chosen to match the spectral shape of the pulse-like accelerograms in the period

range 0.05-6.00s: for each pulse-like record, the spectral-shape-equivalent ordinary one was found by minimizing the sum of squared error differences, allowing for a simple amplitude (linear) scaling factor ≤ 5.
Compared with ordinary far-field records, near-fault pulse-like records tend to cause higher spectral accelerations at longer periods. In particular, the ratio of the pulse period in the ground motion velocity time history to the first-mode period of the building (T_p/T^*) has a critical effect on structural response. For structures responding in the elastic range, the highest demands will be experienced if $T_p \cong T^*$; for ductile structures, the building's effective fundamental period will elongate as damage accumulates. Accordingly, researchers have suggested that ground motion pulses with $T_p \cong 2T^*$may be the most damaging for highly nonlinear systems. For taller buildings where $T_p < T^*$, the pulse period may coincide with higher modes and cause a traveling wave effect over the height of the building, resulting in large displacement and shear force demands in the upper stories.
Based on these considerations, the PL fragility curves are derived using the approach proposed by Champion and Liel [9]. In particular, given the considered fundamental period (T^*) of the archetype building for each considered building class (see Section 4.1), the approach consists of the following steps:

1. Obtain the $Sa_{DS}(T^*)$ values (or simply Sa_{DS}) for which each scaled record reaches the corresponding damage state (DS) threshold in terms of a selected engineering demand parameter (EDP; e.g. maximum inter-story drift);
2. The $ln(Sa_{DS})$ vs. T_p/T^* values for each record are plotted, and an analytical relationship $f(T_p/T^*)$ - polynomial in this study- is fitted to the empirical points. This relationship is taken as the mean value of the logarithm of Sa_{DS}, $\mu_{ln(Sa_{DS})}(T_p/T^*)$;
3. The standard deviation of all the $ln(Sa_{DS})$ values obtained in 1) is calculated;
4. Finally, the PL fragility curves for any DS and T_p/T^* ratio are assumed as lognormal cumulative distribution functions with mean value equal to $\mu_{ln(Sa_{DS})}(T_p/T^*)$ and standard deviation obtained in 3).

The approach used to obtain the NPL fragility curves from the IDA results for the ordinary records can be described as an IM-basis estimation with single-EDP limit states [25].

4. Illustrative application

4.1. Case-study buildings, portfolios and fault

The analysed portfolios are composed by two building typologies representative of distinct vulnerability classes in the Mediterranean region: non-ductile moment-resisting reinforced concrete (RC) infilled frames, mainly designed to sustain gravity loads (i.e. pre-code frames; PI hereinafter); and ductile moment-resisting RC infilled frames designed according to the Eurocode 8 (EC8) seismic provisions for high ductility class (i.e. special-code frames; SI hereinafter). For both building classes, a 4-storey RC moment-resisting frames (MRF) with masonry infills is selected as an index (i.e. archetype) building representative of the common mid-rise buildings in those classes. The PI and SI index buildings were designed by Aljawhari et al. [19], who also developed state-of-the-art OpenSees non-linear models for them as used in this work. The fundamental periods (T_1) of the PI and SI buildings are equal to 0.27s and 0.20s, respectively, while the corresponding bare configurations have periods (T_{bare}) equal to 0.84s and 0.51s, respectively.
Two types of synthetic building portfolios are used in this study, labelled based on their location relative to the fault: a fault-parallel portfolio and a fault-normal one. Both portfolios consist of sites placed in a 1km-spaced uniform grid, with the furthest ones located 84km away from the fault (in the parallel and normal directions), and the closest ones located 5km away from the fault. It is worth noting that 84km corresponds to twice the length of the considered fault (L_{fault}), and a minimum distance of 5km. A graphic representation of the two types of portfolios is shown in Fig. 2. For simplicity, the soil type is assumed to be rock $(V_{s30} = 800\ m/s^2)$. Regarding the distribution of the two building classes within the portfolio, it is assumed that 70% of the buildings at each site are Pre-code structures, while the other 30% are Special-code ones.
For illustrative purposes, a strike-slip fault capable of generating a magnitude $M_{w,char} = 7.0$ characteristic earthquake, according to the characteristic earthquake model described by Schwartz and Coppersmith [26], is chosen for this study. The model considers a log lineal recurrence relationship (i.e. relationship between the

frequency of occurrence and the magnitude of earthquakes) for moderate events, and a constant probability of occurrence for events with magnitudes around $M_{w,char}$. A minimum magnitude of $M_{w,min} = 5.0$ and a b constant (ratio between small and large events) of one are assumed for the assessment. The fault length and the magnitude-dependent rupture lengths are obtained using the equations proposed by Wells and Coppersmith [26], and uniformly distributed epicentre distances along the fault are assumed for the simulation.

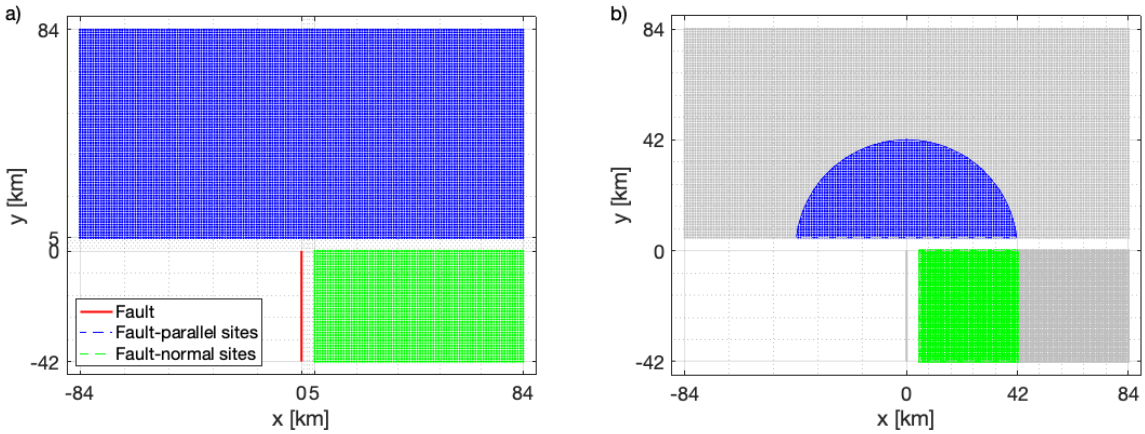

Fig. 2 – a) Fault-parallel and fault-normal portfolio types; b) Example of portfolios for $r_{jb} \leq 42\ km$.

4.2. Results and discussion

The hazard curves are obtained for three representative sites in each portfolio, with Joyner-Boore distance r_{jb} (i.e. the shortest distance from a site to the surface projection of the rupture surface) values of 5km, 21km ($L_{fault}/2$), and 42 km (L_{fault}) respectively, and are shown in Fig. 3. It is important to mention that the spectral acceleration values obtained from the assessment correspond to $Sa(T_{bare})$.

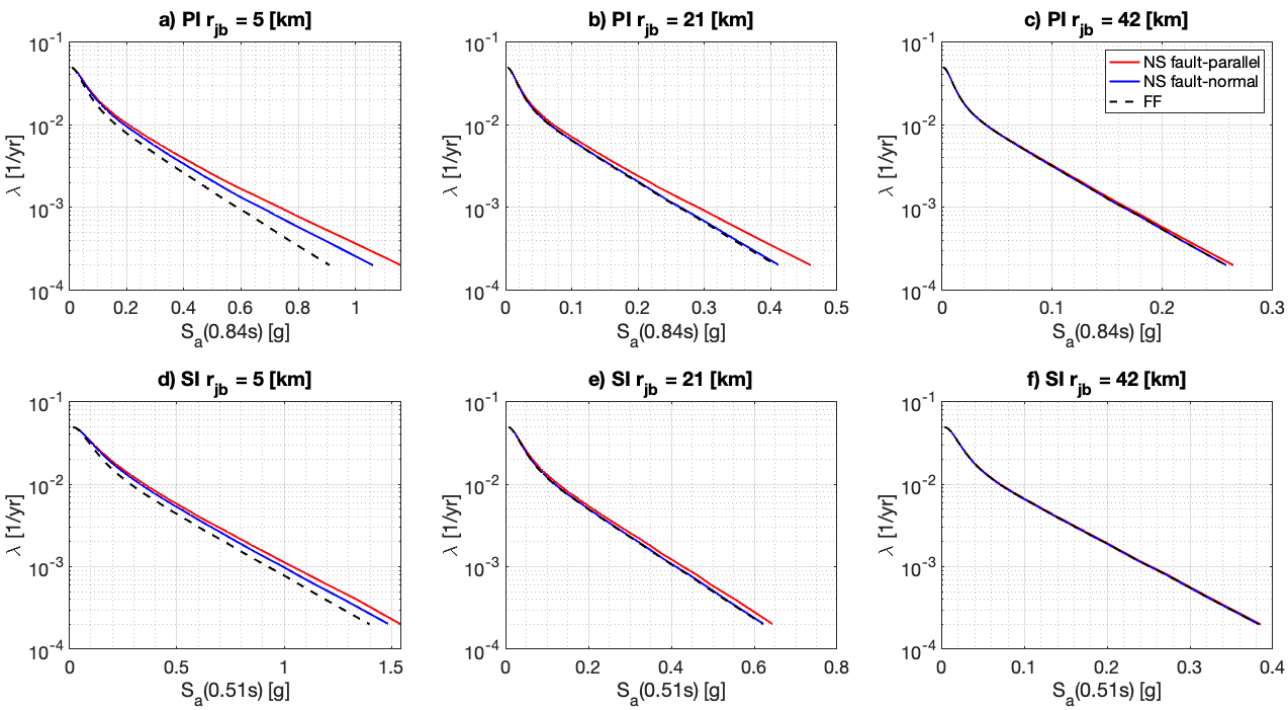

Fig. 3 – Hazard curves for sites located at 5, 21, and 42 km from the fault

It can be seen from Fig. 3 that the spectral amplification due to forward-directivity is less significant for sites that are farther away from the fault, as expected due to the lower probability of pulse occurrence at those sites. It is also interesting noting that, for the same r_{jb} values, the sites located in the fault-parallel region experience a much higher spectral amplification when compared to the ones in the fault-normal region. It can also be seen that spectral amplification is significantly higher for PI buildings, reaching an amplification of 21% and 17% for 475 and 2,475 years of return period, respectively, which almost double the corresponding values for SI structures. Fig. 4 provides a better visualization of the spatial distribution of spectral amplification for the 475 and 2,475 return periods.

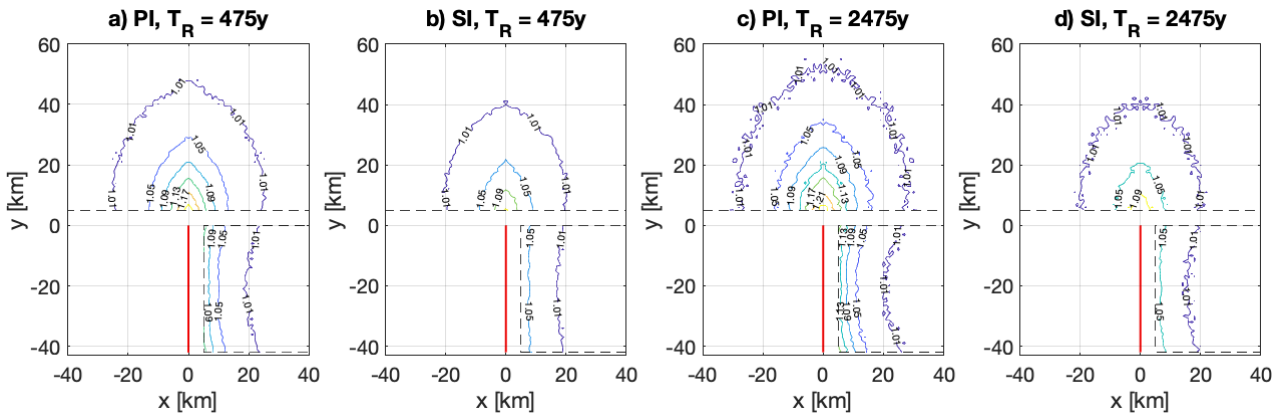

Fig. 4 – Spatial distribution of spectral amplification for $T_R = 475$y and 2475y.

The results of the hazard assessment and the fragility curves described in section 3 are finally used to perform the loss assessment for the two portfolios. The AAL values are obtained for portfolios of different sizes, characterized by the maximum r_{jb} value of their farther sites, $r_{jb_{max}}$. An example of the fault-parallel and fault-normal portfolios considered for all $r_{jb_{max}} = 42\ km$ is shown in Fig. 2.

The AAL amplification values due to forward-directivity effects are shown in Fig. 5, along with their spatial distribution. The amplification for the fault-parallel and fault-normal portfolios with $r_{jb} = 5\ km$ are 19% and 11%, respectively. The fault-parallel portfolios exhibit a drastic decrease of the AAL figures when increasing the $r_{jb_{max}}$. For $r_{jb_{max}} = 30\ km$, it can be seen that the amplification expected for both portfolios is the same (around 4%). However, these results should be taken with caution, as the $r_{jb_{max}}$ does not work in the same way for the portfolios; when increasing the value of $r_{jb_{max}}$, the proportion of buildings that are farther away from the fault increases significantly faster in the case of the fault-parallel portfolio when compared to the fault-normal one. This is due to the semi-circle and rectangular forms of the fault-parallel and fault-normal portfolios, respectively.

Fig. 5 shows that, for a maximum distance of 25 km, the amplification of the AAL due to the directivity-induced pulse-like ground motions is under 5% for both portfolios, which could be considered as a threshold to decide whether to include the pulse-like effects in the loss assessment exercise.

5. Conclusions

In this study, a probabilistic risk modelling approach was used to investigate the influence of near-source directivity effects on the expected loss for building portfolios. The simulations were performed for two portfolios consisting of Pre-code and Special-code frame buildings, located in the fault-parallel and fault-normal directions near a strike-slip fault.

The results obtained from the hazard module for near-source and far-field conditions show significantly higher amplification of the spectral acceleration due to near-source directivity effects for the fault-parallel portfolio when comparing sites with the same r_{jb} in the fault-normal region. A maximum spectral amplification of 21% is reached for the $T_R = 2{,}475$ years hazard for a PI building located at 5 km distance in the fault-parallel

direction. However, that figure decreases to only 1% for a site located at a distance equivalent to L_{fault} in the fault-parallel direction, and $L_{fault}/2$ in the fault-normal direction, regardless of the building class or the return period.

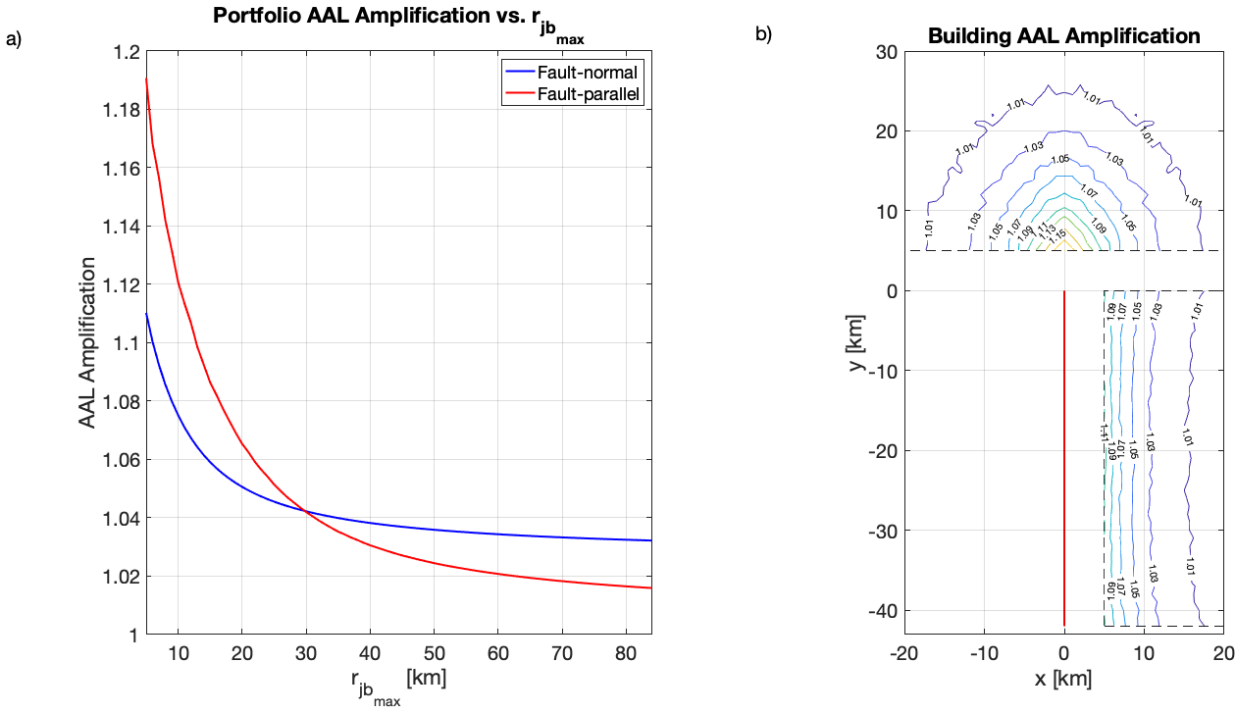

Fig. 5 – (a) AAL values and amplification factors of the portfolios depending on their $r_{jb_{max}}$; (b) spatial distribution of AAL amplification

Regarding the expected loss, when pulse-like ground motions were considered, maximum amplifications of 19% and 11% were obtained for the AAL values when compared to far-field conditions for sites located 5 km away from the fault in the fault-parallel and fault-normal directions, respectively. Those figures drop drastically as the distance increases, reaching values of around 1% amplification for sites located 25 km away from the fault.

The expected losses were also studied for different sized portfolios, characterized by their maximum r_{jb} value. In this case, the figures go from 19% of AAL amplification for the buildings that are closer to the fault, to only 5% for portfolios with a maximum r_{jb} of 25 km. These results show that the influence of near-source directivity effects is significant when estimating the losses of individual building or small portfolios located very close to a fault. Nevertheless, the impact of pulse-like ground motions on the losses of larger portfolios can be considered minimal.

References

[1] Somerville PG, Smith NF, Graves RW, Abrahamson NA (1997): Modification of empirical strong ground motion attenuation relations to include the amplitude and duration effects of rupture directivity. *Seismological Research Letters*, **68**:199–222.

[2] Bray JD, Rodriguez-Marek A (2004): Characterization of forward-directivity ground motions in the near-fault region. *Soil Dynamics and Earthquake Engineering*, **24**:815–28.

[3] Baker JW, Cornell CA (2008): Vector-valued intensity measures for pulse-like near-fault ground motions. *Engineering Structures*, **30**:1048–57.

[4] Spudich P, Bayless JR, Baker J, Chiou BSJ, Rowshandel B, Shahi S, et al. (2013): Final Report of the NGA-West2 Directivity Working Group. *Pacific Engineering Research Center Report*,:162.

[5] Shahi SK, Baker JW (2011): An empirically calibrated framework for including the effects of near-fault directivity in probabilistic seismic hazard analysis. *Bulletin of the Seismological Society of America*, **101**:742–55.

[6] Chioccarelli E, Iervolino I (2013): Near-source seismic hazard and design scenarios. *Earthquake Engineering & Structural Dynamics*, **42**:603–22.

[7] Chopra AK, Chintanapakdee C (2001): Comparing response of SDF systems to near-fault and far-fault earthquake motions in the context of spectral regions. *Earthquake Engineering and Structural Dynamics*, **30**:1769–89.

[8] Alavi B, Krawinkler H (2004): Behavior of moment-resisting frame structures subjected to near-fault ground motions. *Earthquake Engineering and Structural Dynamics*, **33**:687–706.

[9] Champion C (2010): The effect of near-fault directivity on building seimic collapse risk. university of colorado.

[10] Yepes-Estrada C, Silva V, Rossetto T, D'Ayala D, Ioannou I, Meslem A, et al. (2016): The global earthquake model physical vulnerability database. *Earthquake Spectra*, **32**:2567–85.

[11] Mitchell-Wallace K, Jones M, Hillier J, Foote M (2017): Natural catastrophe risk management and modelling. Wiley, New York; .

[12] Baker JW (2007): Quantitative classification of near-fault ground motions using wavelet analysis. *Bulletin of the Seismological Society of America*, **97**:1486–501.

[13] Chiou B, Darragh R, Gregor N, Silva W (2008): NGA project strong-motion database. *Earthquake Spectra*, **24**:23–44.

[14] Iervolino I, Cornell CA (2008): Probability of occurrence of velocity pulses in near-source ground motions. *Bulletin of the Seismological Society of America*, **98**:2262–77.

[15] Somerville PG (2003): Magnitude scaling of the near fault rupture directivity pulse. *Physics of the Earth and Planetary Interiors*, **137**:201–12.

[16] Boore DM, Atkinson GM (2008): Ground-motion prediction equations for the average horizontal component of PGA, PGV, and 5%-damped PSA at spectral periods between 0.01 s and 10.0 s. *Earthquake Spectra*, **24**:99–138.

[17] Assatourians K, Atkinson GM (2013): EqHaz: An Open-Source Probabilistic Seismic-Hazard Code Based on the Monte Carlo Simulation Approach. *Seismological Research Letters*, **84**:516–24.

[18] Di Pasquale G, Orsini G, Romeo RW (2005): New developments in seismic risk assessment in Italy. *Bulletin of Earthquake Engineering*, **3**:101–28.

[19] Aljawhari K, Freddi F, Galasso C (2019): State-dependent vulnerability of case-study reinforced concrete frames. Soc. Earthq. Civ. Eng. Dyn.

[20] Federal Emergency Management Agency (2012): Seismic Performance Assessment of Buildings. Volume 1 - Methodology. Washington, DC: .

[21] Risk management solutions (2008): A Guide to catasrophe modelling. *The Review*, **09**.

[22] Kohrangi M, Vamvatsikos D, Bazzurro P (2019): Pulse-like versus non-pulse-like ground motion records: Spectral shape comparisons and record selection strategies. *Earthquake Engineering and Structural Dynamics*, **48**:46–64.

[23] Shahi SK, Baker JW (2014): An efficient algorithm to identify strong-velocity pulses in multicomponent ground motions. *Bulletin of the Seismological Society of America*, **104**:2456–66.

[24] Ancheta TD, Darragh RB, Stewart JP, Seyhan E, Silva WJ, Chiou BSJ, et al. (2014): NGA-West2 database. *Earthquake Spectra*, **30**:989–1005.

[25] Bakalis K, Vamvatsikos D (2018): Seismic Fragility Functions via Nonlinear Response History Analysis. *Journal of Structural Engineering (United States)*, **144**:1–15.

[26] Schwartz DP, Coppersmith KJ (1984): Fault behavior and characteristic earthquakes: examples from the Wasatch and San Andreas fault zones (USA). *Journal of Geophysical Research*, **89**:5681–98.

